InAs quantum dot infrared photodetectors with $In_{0.15}Ga_{0.85}As$ strain-relief cap layers

Zhengmao Ye and Joe C. Campbell[a)]
Microelectronics Research Center, University of Texas at Austin, Building 160, 10,100 Burnet Road, Austin, Texas 78712

Zhonghui Chen, Eui-Tae Kim, and Anupam Madhukar
Department of Materials Science and Physics, University of Southern California, Los Angeles, California 90089

(Received 1 April 2002; accepted 9 September 2002)

We report InAs quantum dot infrared photodetectors that utilize $In_{0.15}Ga_{0.85}As$ strain-relief cap layers. These devices exhibited normal-incidence photoresponse peaks at 8.3 or 8.8 μm for negative or positive bias, respectively. At 77 K and -0.2 V bias the responsivity was 22 mA/W and the peak detectivity D^* was 3.2×10^9 cm $Hz^{1/2}$/W. © *2002 American Institute of Physics.*
[DOI: 10.1063/1.1517750]

I. INTRODUCTION

As a potential candidate for mid-infrared (3–5 μm) and far-infrared (8–14 μm) photon detection, the quantum dot infrared photodetector (QDIP) has been the subject of extensive research efforts in recent years. Normal-incidence QDIPs with *n-n-n*[1–4] and *n-i-n*[5–10] vertical configurations have been reported. Compared with quantum well infrared photodetectors, QDIPs are sensitive to normal-incidence infrared radiation owing to three-dimensional confinement of the electrons in the quantum dots, a characteristic that is advantageous for focal plane arrays. In addition, due to greatly suppressed electron–phonon scattering, QDIPs have the advantages of low dark current and long carrier lifetimes, which establish the potential for high temperature operation. Furthermore, photoconductive gain that ranges from unity to several thousand has been reported.[6,11,12] Normal-incidence QDIPs with encouraging performance at ~77 K have been demonstrated from 3 to 14 μm wavelength. In the mid-wavelength infrared (MWIR) regime, we demonstrated a peak detectivity D^* of 1.5×10^9 cm $Hz^{1/2}$/W at 7.2 μm at 77 K in Al-free GaAs(001)/InAs *n-i-n* QDIPs.[5,6] To improve upon the dark current and D^*, the notion of a current blocking AlGaAs layer in the otherwise GaAs confinement layers has been proposed.[13] With such an AlGaAs current blocking layer, a peak D^* at 3.7 μm of 3×10^9 cm $Hz^{1/2}$/W at 100 K in *n-n-n*[2] and a peak D^* at 6.2 μm of 10^{10} cm $Hz^{1/2}$/W at 77 K in *n-i-n*[6] have been achieved in GaAs(001)/InAs QD based QDIPs. In the long-wavelength infrared (LWIR) regime, a QDIP based on GaAs(001)/InGaAs QDs in *n-n-n* structure with a peak D^* at 13 μm of 2×10^8 cm $Hz^{1/2}$/W at 78 K has been demonstrated.[1] Recently, we have demonstrated the first normal-incidence bias-controlled tunable mid (~5.6 μm) and long (~10 μm) wavelength infrared (IR) photoresponse in a QDIP structure.[8,14] This *n-i-n* structure is based on InGaAs capped GaAs(001)/InAs quantum dots with two different quantum dot size distributions. Its 77 K peak detectivities at mid (~5.6 μm) and long (~10 μm) wavelength are 5.8×10^9 and 7.3×10^8 cm $Hz^{1/2}$/W, respectively.[14] In the long-wavelength infrared regime ($\lambda>8$ μm), all reported normal-incidence peak detectivities of QDIPs (with contacts in the vertical configuration) are, so far, below 10^9 cm $Hz^{1/2}$/W at ~77 K. Recently, we have realized[9] a narrow, essentially unimodal, QDIP intraband photoresponse at 8–9 μm with a similar structure based on $In_{0.15}Ga_{0.85}As$ capped GaAs(001)/InAs QDs having an essentially unimodal QD size distribution.[9] In this article we report on the photodetector characteristics of this structure. These devices have achieved low dark current, low noise, and high detectivity at 8–9 μm and 77 K.

II. EXPERIMENTAL RESULTS

A. Device structure

The InAs QDIP studied in this work belongs to the class of *n-i-n* structure QDIPs under examination by us.[5–10,13–15] Figure 1(a) shows a schematic of the QDIP structure. The sample was grown on semi-insulating GaAs (001) substrates by solid-source molecular beam epitaxy. Five layers of nominally 2.0 monolayer (ML) InAs at a growth rate of ~0.22 ML/s at ~500 °C were inserted between highly Si-doped top and bottom GaAs contact layers. Then 20 ML $In_{0.15}Ga_{0.85}As$ regions were grown via migration enhanced epitaxy (MEE) at ~350 °C as the quantum dot cap layers followed by 20 ML of MEE grown GaAs. Additional 160 ML of GaAs was grown via molecular beam epitaxy at 500 °C for a total of 180 ML GaAs spacer layers. The GaAs layers between the contact layers and the nearest quantum dot layer had a thickness of 220–240 MLs.

Devices were fabricated from pieces of the same as-grown sample as reported in Ref. 9 and followed standard procedure: photolithography, wet chemical etching, metal deposition and liftoff, and rapid thermal annealing. Photolithography and wet chemical etching were used to define the device mesas, which had a diameter of 250 μm and a height

a)Author to whom correspondence should be addressed; electronic mail: zmye@mail.utexas.edu

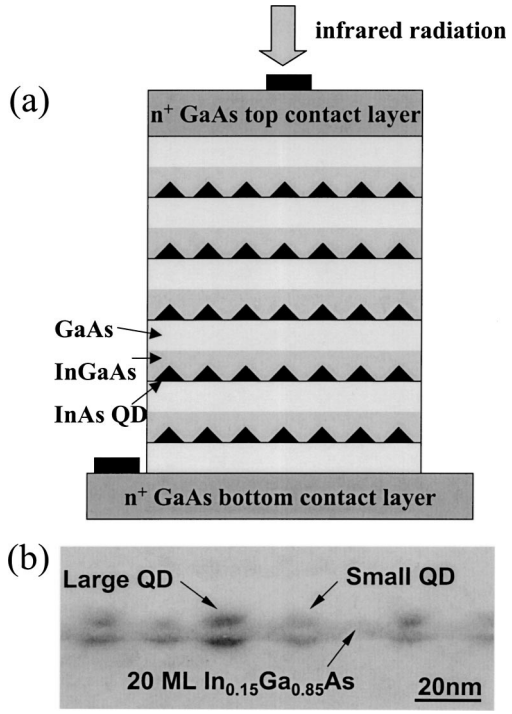

FIG. 1. (a) Schematic of an InAs/$In_{0.15}Ga_{0.85}As$/GaAs quantum dot infrared photodetector structure. (b) Cross-sectional transmission electron microscopy image (dark field, $\mathbf{g}=[002]$, [110] azimuth) of the quantum dots.

of ~1.4 μm. Electron beam deposition of AuGe/Ni/Au and liftoff were then performed to form the top and bottom contacts. This was followed by a rapid thermal anneal at 430 °C for 20 s in nitrogen. In the following discussion, ''positive'' bias means that a positive voltage was applied to the top contact.

The typical average height of the QDs is ~3.5 nm, as derived from atomic-force microscopy measurements on a counterpart uncapped sample. Figure 1(b) shows a typical cross-sectional transmission-electron-microscope (X-TEM) image of the $In_{0.15}Ga_{0.85}As$-capped 2 ML GaAs(001)/InAs QDs. The image clearly shows that the typical base dimension of the QDs is ~20 nm, which is nearly four times smaller than the exciton radius (~75 nm) of bulk InAs. The electronic states of regions with such small lateral dimensions have thus a strong lateral confinement effect on the excitonic luminescence: thus identified as QD at least for the electronic ground states. This is further confirmed by the photoluminescence (PL) excitation (PLE) spectrum of the QDIP sample (shown in Fig. 2, with detection energy of 1.125 eV which is the peak energy of its PL spectrum). The steplike PLE feature at 1.34 eV arises from the GaAs/InGaAs/GaAs QW region between the InAs QDs, reflecting the step-like state density of QWs with one-dimensional confinement. The PLE peak at ~1.21 eV reflects the discrete (delta function like) state density broadened by the inhomogeneity of QD sizes. This peak arises from the InGaAs capped InAs QDs, not from the GaAs/InGaAs/GaAs QW. Thus, both X-TEM and PLE data indicate that the InGaAs-capped InAs QDs have three-dimensional confinement and delta function like discrete state density, at least for the electron ground states. Such states are the initial states of the observed intraband photoresponses of the QDIPs discussed in the following section.

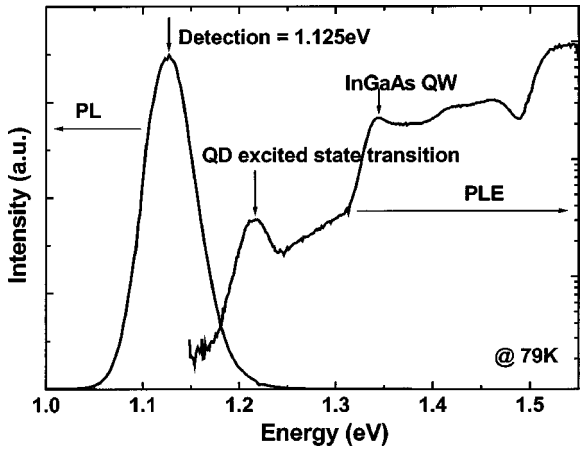

FIG. 2. 79 K PL and PLE spectra of the quantum dot infrared photodetector structure.

B. Photocurrent spectra and responsivity

The normal-incidence spectral response of the *n-i*(QDs)-*n* QDIPs was measured with a Nicolet Magna-IR 570 Fourier transform IR (FTIR) spectrometer and a SRS 570 low- noise current preamplifier. In order to rule out parallel propagation of light reflected from the mesa sidewall, we measured the spectral response of the QDIPs with metal defined opening on the top of the mesa, whose diameter (220 μm) was smaller than that of the mesa (250 μm). By using this metal cover, the parallel propagating light reflected off from the detector mesa sidewall was negligible. The spectral response demonstrated no significant change of the peak wavelength and the magnitude of the photocurrent, which suggested that the photocurrent arising from the light reflected from the mesa sidewall did not significantly affect the photoresponse. The photoresponse was also measured with two orthogonal linear polarizations. No polarization dependence was observed. These results indicate that the QDIP photocurrent arises from normally incident radiation. Figure 3(a) shows the spectral response at 77 K for bias voltages in the range 0–0.8 V. The intraband photoresponse peak occurred at ~8.8 μm (141 meV) for bias larger than 0.2 V. At $\leqslant$0.1 V [see inset, Fig. 3(a)] the photoresponse is weak but peaked at 5.4 μm (230 meV) with a smaller peak at ~8.8 μm. At zero bias (photovoltaic mode), only a weak response at 5.4 μm was observed. We note that the conduction band bandoffset for the GaAs/$In_{0.15}Ga_{0.85}As$/GaAs QWs is estimated in the literature to be 145 ± 15 meV. Although this value is close to the 8.8 μm (141 meV) photoresponse, this response (more precisely, 8.22 μm at -0.8 V) does not arise from the GaAs/20 ML $In_{0.15}Ga_{0.85}As$/GaAs QW regions between the InAs QD regions. This is supported by our early reported experimental data[10] on infrared detector structures that contain a wider GaAs/30 ML $In_{0.15}Ga_{0.85}As$/GaAs QW regions between QDs, and show a redshift (from the 8.22 μm response of the current GaAs/20 ML $In_{0.15}Ga_{0.85}As$/GaAs containing sample) to 9.3 micron (at

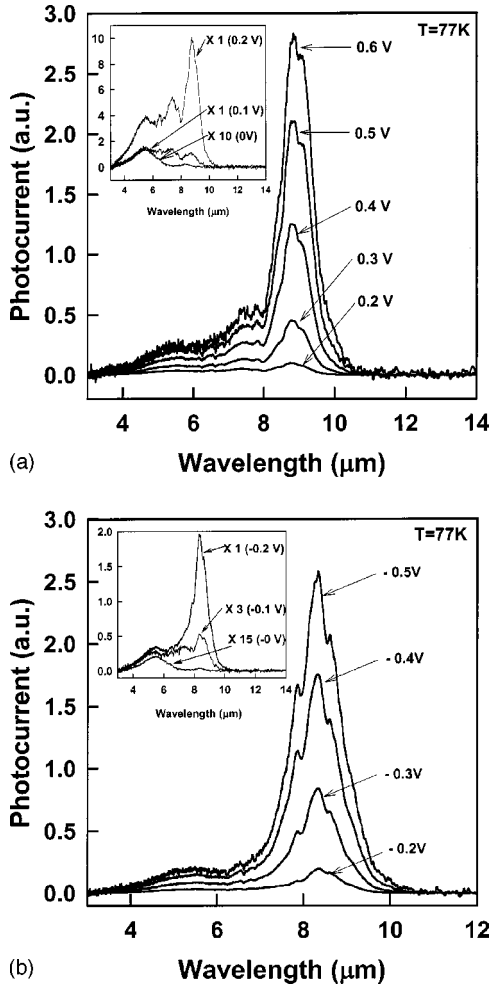

FIG. 3. Normal-incidence spectral response at positive (a) and negative (b) bias and 77 K measured with a FTIR spectrometer. The inset shows photovoltaic operation and the spectral responses at ± 0.2 and ± 0.1 V.

-0.8 V) for the 8.8 μm photoresponse. This is in contrast to the blueshift that should result if the origin of this photoresponse peak were in the QW region between the QDs. Thus, the 8.8 μm photoresponse arises from the InAs QDs. Considering that the barrier height of $In_{0.15}Ga_{0.85}As/GaAs$ is about 145 meV, the much smaller 5.4 μm ($\sim$230 meV) photoresponse clearly arises from the InAs QDs. Thus, both the 8.8 and 5.4 μm photoresponses arise from the InAs QDs.

As noted above, previously we have observed voltage-controllable MWIR (5.6 μm) and LWIR (9.3 μm) response peaks in QDIPs with explicit bimodal quantum dot size distributions.[8,10,14] The presence of the two peaks and the change in the relative response with bias was attributed to differences in the population of the ground states of the ''large'' and ''small'' quantum dots for different bias voltages. It should be noted that the nature of the intraband photocurrent in QD structures is complex due to convolution of the transition matrix elements, density of final states, and weighted photocurrent extraction barriers. Consequently, it is not possible to make unambiguous correlation between quantum dot ''size'' and photocurrent peak response. While the current QDIPs do not exhibit an explicit bimodal QD size distribution, the tail of the unimodal distribution nevertheless

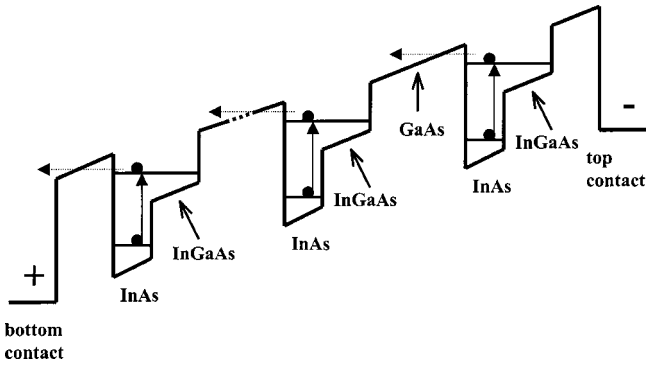

FIG. 4. Schematic of the band structure.

comprises a small percentage of larger QDs. These QDs have a lower ground state energy and, in our *n-i*(QDs)-*n* structures, higher electron occupation at zero and low bias. Hence the weak 5.4 μm response is dominant at zero and very low bias. At higher bias, occupation shifts to smaller QDs. The photovoltaic behavior of these QDIPs is due to intraband-transition induced dipole moments in QDs.[15] The dipole moments originate in the asymmetric confining potential along the growth direction that results from the pyramidal-shaped InAs quantum dots, the $In_{0.15}Ga_{0.85}As$ cap layers on the top of the quantum dots, and the wetting layers underneath the quantum dots. Note that the full width half maximum (FWHM) $\Delta\lambda$ of the $\sim$8.8 μm peak is $\sim$1.0 μm and $\Delta\lambda/\lambda$ is $\sim$12%. In the photovoltaic mode, the FWHM of the 5.4 μm peak is 1.6 μm and $\Delta\lambda/\lambda = 30\%$. This spectral width being broader suggests that the larger QDs in the broad tail of the QD size distribution are responsible for this peak, potentially through the participation of bound-to- quasi-continuum intraband transitions. Moreover, as noted here earlier and also discussed in detail in Ref. 9, the initial states for the observed 8.8 and 5.4 μm photoresponses correspond to the bound QD electron ground states. The final states of the observed 8.8 and 5.4 μm photoresponses are likely a mixture of the InAs QD and GaAs/InGaAs/GaAs QW states, and thus have progressively more laterally extended nature with increasing transition energy.

The band diagram under negative bias is shown schematically in Fig. 4. For negative bias, the photoresponse peak shifted to 8.3 μm, a manifestation of the asymmetric band diagram described above. The FWHM was $\sim$0.9 μm at -0.2 V and increased to 1.2 μm at -0.5 V. The corresponding values of $\Delta\lambda/\lambda$ were 11% and 14%, respectively. The photocurrent increased significantly with voltage for both positive and negative bias because the resulting increase in dark current populated the quantum dot ground states. These electrons participated in the infrared photon absorption and contributed to the photocurrent.

The absolute spectral responsivity was calibrated with a blackbody source ($T = 995$ K). Figure 5 shows the peak responsivity versus bias at temperatures of 77, 100, and 120 K. An optical band-pass filter with a transmission window from 7.0 to 14.5 μm was placed next to the aperture of the blackbody to block the shorter wavelength radiation. This is particularly important for $\lambda < 3$ μm, which could result in inter-

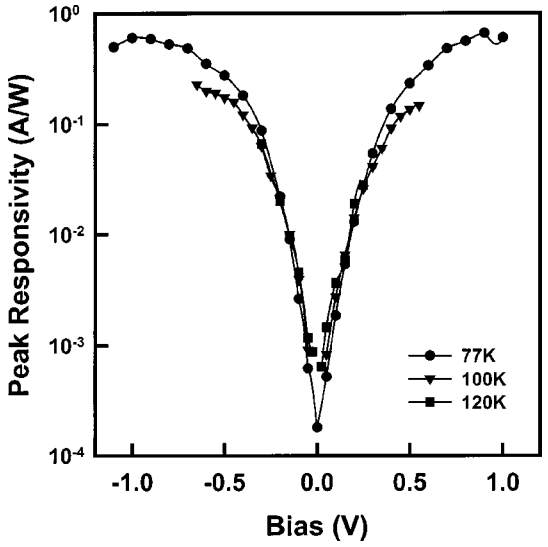

FIG. 5. Absolute peak responsivities measured at 77, 100, and 120 K. The responsivities were determined using a blackbody source.

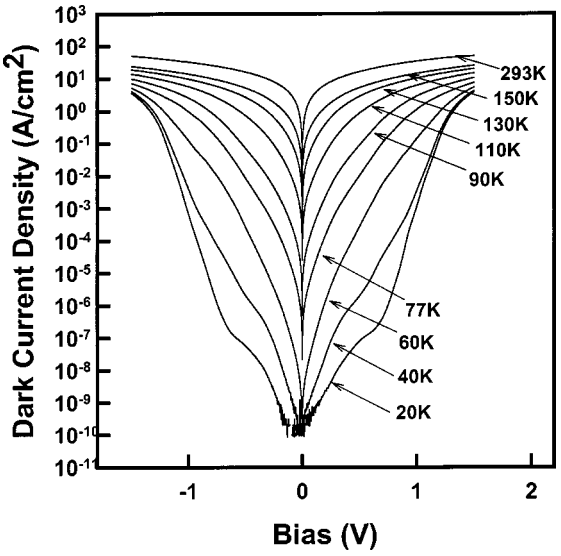

FIG. 6. Dark current density vs bias curves for temperature in the range from 20 to 293 K.

band transitions that would significantly alter the photocurrent. At 77 K, with increase in positive bias, the responsivity increased from 13 mA/W at 0.2 V to 660 mA/W at 0.9 V. For negative bias, the responsivity increased from 22 mA/W at -0.2 V to 600 mA/W at -0.9 V. The different responsivity curves for the positive and negative bias are due to the asymmetric band structure; electrons in the quantum dots experience different barrier heights depending on whether transport is toward the top or bottom contacts. Negative differential responsivity was observed with further increase in voltage, for both the positive and negative bias cases. This could be a result of ''overfilling'' the quantum dots, i.e., the higher dark currents that are concomitant with higher bias populate the higher states in the quantum dots and thus reduce the probability for intraband transitions. At low bias ($|V| \leqslant 0.1$ V), the photocurrent increased with temperature. This is due to the fact that the electrons fill more of the ground states in the quantum dots. However, at higher bias, the photocurrent decreased with temperature, which could be a result either of overfilling, which occurs at lower voltage with increasing temperature, or of a decrease in lifetime of photoexcited electrons due to an enhanced electron–phonon scattering.

C. Dark current, noise, and optical gain

Figure 6 shows the dark current density versus voltage characteristics for temperature in the range 20–296 K. The structural asymmetry, discussed above, also resulted in asymmetric dark current density for positive and negative bias. As the temperature increased from 20 K to room temperature, the dark current density increased over 10 orders of magnitude from 9.5×10^{-9} to 9.6 A/cm^2 at 0.3 V and from 6.2×10^{-9} to 9.6 A/cm^2 at -0.3 V. At low bias, the increase in dark current density at low temperature was due to the fact that as the bias increased, more electrons occupied the quantum dots, which resulted in an increase in the average sheet electron density. When a large fraction of the quantum dot states are occupied, further increase in bias does not significantly alter the sheet electron density. This caused a lowering of the energy barrier for injected electrons at the contact layers, which resulted in the nearly exponential increase of the dark current. The logarithm of the dark current density versus inverse temperature ($1000/T$) is plotted (0–1 V) in Fig. 7 and Fig. 8 (-0.1 V). At -0.1 V, excellent linear fits were obtained over 7 orders of magnitude for temperature higher than 77 K. The exponential increase in the dark current suggests that carrier thermal excitation to higher energy states is involved. For temperature lower than 77 K, the dark current density is relatively insensitive to temperature, an attribute of phonon assisted tunneling and sequential resonant tunneling. From Fig. 8, we can extract an activation energy of 135 meV. This is, interestingly, essentially the same as the FTIR measured cutoff energy $E_c = 138$ meV (wavelength of 9 μm). This coincidence indicates the at zero

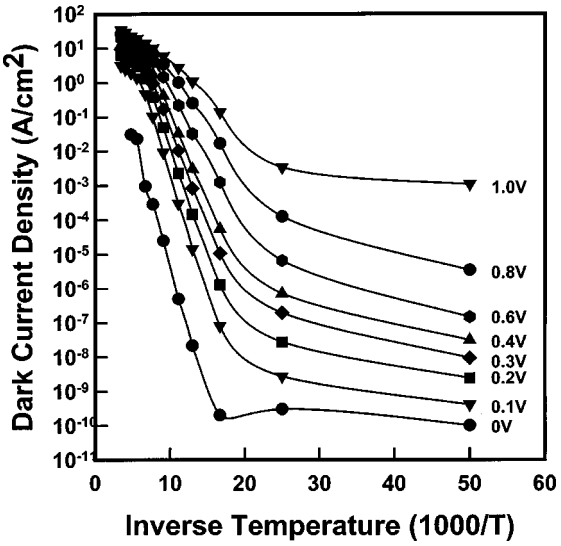

FIG. 7. Dark current density vs inverse temperature for 20 K$\leqslant T \leqslant$293 K. Each curve represents dark current density at fixed bias.

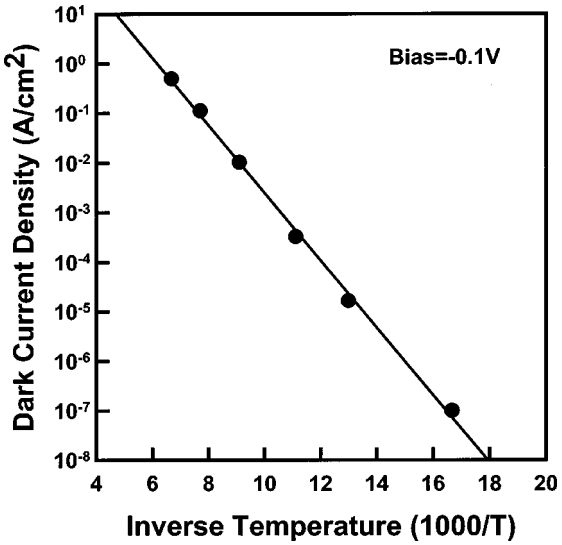

FIG. 8. Dark current density vs inverse temperature. The slope gives an activation energy of $E_a = 135$ meV.

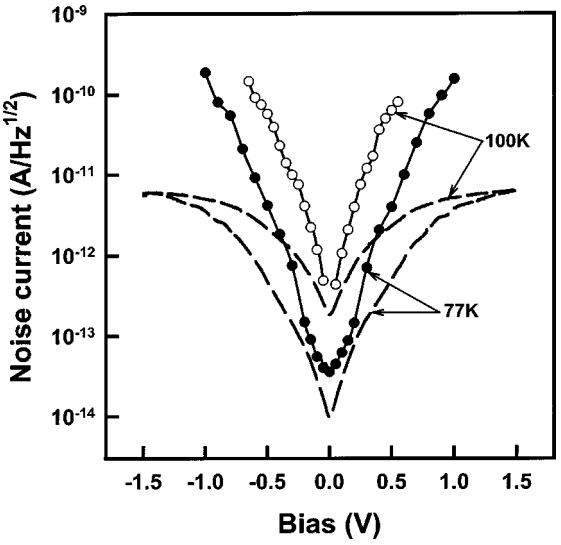

FIG. 10. Measured noise current vs bias at 77 and 100 K. The dashed lines shows calculated thermal noise current at 77 and 100 K.

bias the dark current is carried through thermal activation to the same excited states of QD as participating in the absorption and subsequent rapid tunneling. The activation energy decreased linearly with bias, as shown in Fig. 9. At high bias, the activation energy was close to kT, which resulted in high dark current even at low temperature. Compared to a similar structure with 2.5 ML InAs quantum dots and 30 ML $In_{0.15}Ga_{0.85}As$ cap layers, the dark current density was 1 order of magnitude higher.[8–10,14] This increase in the dark current results from the reduction of the thickness of the $In_{0.15}Ga_{0.85}$ cap layers and from the decrease in binding energy of the ground states.

The dark current noise current i_n was characterized with low noise current preamplifiers and a SRS 760 fast Fourier transform spectrum analyzer. Figure 10 shows the noise current of a 250-μm-diam device at 77 K (solid circles) and 100 K (open circles) versus bias voltage. For low bias, i.e., $|V_B| < 0.1$ V, the measurement was limited by the noise floor of the instruments. The calculated thermal noise current I_{th} at 77 and 100 K is also shown. The thermal noise current can be expressed as

$$I_{\text{th}} = \sqrt{\frac{4kT}{R}},$$

where k is Boltzmann's constant, T is the absolute temperature, and R is the differential resistance of the device, which was extracted from the slope of dark current. At $V_B = 0.1$ V and 77 K, the calculated thermal noise current (3×10^{-14} A/Hz$^{1/2}$) was close to the measured noise current (6×10^{-14} A/Hz$^{1/2}$), indicating that thermal noise is significant in the low bias region. As the bias increased, the noise current increased much faster than thermal noise. The noise current at high bias ($|V_B| > 0.1$ V) appeared to be generation-recombination (GR) noise. Combining the noise current with the dark current, the photoconductive gain G was calculated using the relation

$$G = \frac{i_n^2}{4eI_d},$$

where I_d is the dark current. Figure 11 shows the photoconductive gain of a 250-μm- diameter device at 77 and 100 K for positive and negative bias. At 77 K, gain increased exponentially with bias at low voltage, saturated in a narrow bias range, i.e., $-0.4 - -0.5$ V, and then increased exponentially with bias.

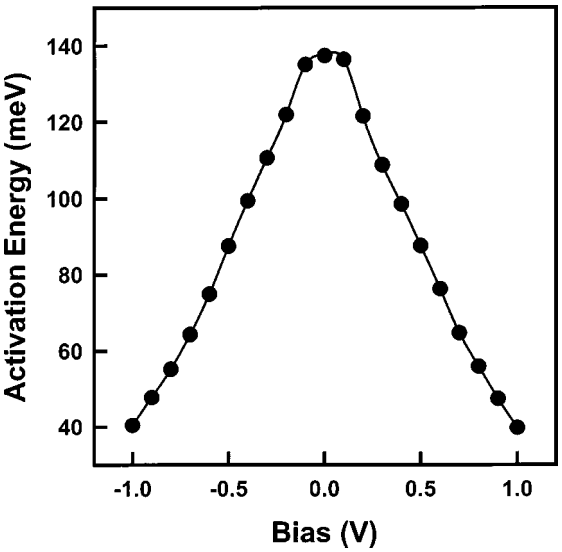

FIG. 9. Dark current activation energy vs bias.

D. Quantum efficiency and detectivity

The external quantum efficiency η_{ext} is the ratio of the number of countable output carriers to the number of incident photons. η_{ext} can be expressed as follows:

$$\eta_{\text{ext}} = \frac{I_{\text{ph}}/e}{P_{\text{in}}/h\frac{c}{\lambda}} = R \cdot \frac{hc}{\lambda e},$$

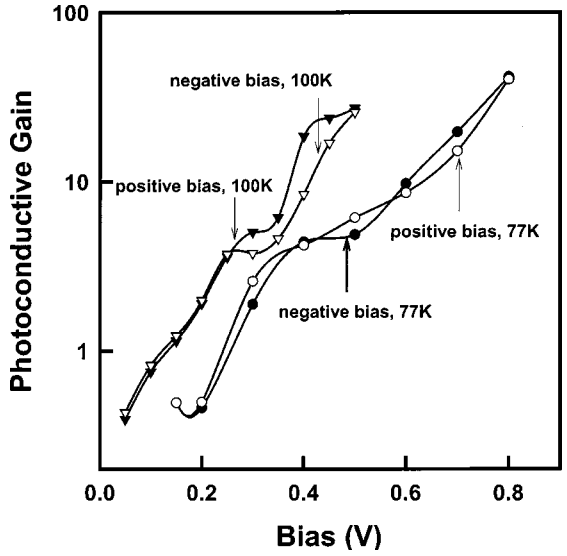

FIG. 11. Photoconductive gain vs bias at 77 and 100 K.

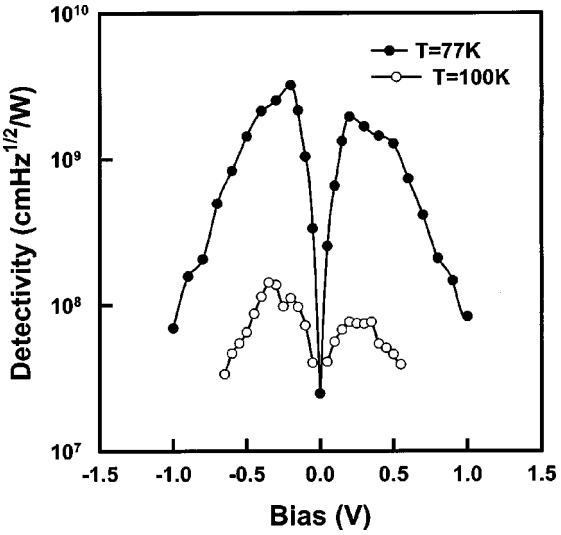

FIG. 13. Detectivity vs bias at 77 and 100 K.

where I_{ph} is the photocurrent, P_{in} is the input power, λ is the peak wavelength, and R is the peak responsivity. Figure 12 shows the quantum efficiency versus bias at 77 K. With increase in bias, η_{ext} increased linearly and then saturated at high bias reaching a maximum value of $\eta_{\mathrm{ext}} \approx 9\%$. The internal quantum efficiency η_{int} can be estimated by using the relation

$$\eta_{\mathrm{int}} = \frac{\eta_{\mathrm{ext}}}{G \cdot (1-R)},$$

where R (8.8 μm)=28% is the reflectivity of the GaAs contact layers. At low bias, η_{int} increased with bias due to filling of the ground states. However, at high bias, η_{int} slowly decreased due to the overfilling effect discussed above.

The detectivity is given by

$$D^* = \frac{R\sqrt{A \cdot \Delta f}}{i_n},$$

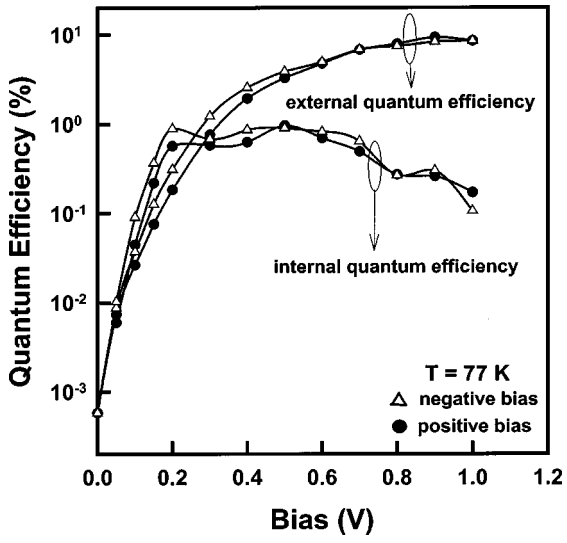

FIG. 12. Internal and external quantum efficiency vs bias at 77 K.

where A is the device area, R is the responsivity, i_n is the noise current, and Δf is the bandwidth. Figure 13 shows the peak detectivity for the 8.3 and 8.8 μm peaks at 77 and 100 K. The best performance was achieved at 77 K and -0.2 V where the peak detectivity was 3.2×10^9 cm Hz$^{1/2}$/W. The corresponding responsivity was 22 mA/W. Note the rapid decrease of the detectivity with the increase in temperature for both peaks. Owing primarily to the rapid increase in GR noise current at 100 K, the detectivity of the 8.3 μm peak dropped to 1.5×10^8 cm Hz$^{1/2}$/W at -0.35 V.

III. SUMMARY

In summary, we have demonstrated InAs/InGaAs/GaAs QDIPs with strain relief $In_{0.15}Ga_{0.85}As$ cap layers. These QDIP exhibited photoresponse peaks at 8.3 μm (negative bias) or 8.8 μm (positive bias). At 77 K, the low dark current and responsivity of 22 mA/W yielded a peak D^* of 3.2×10^9 cm Hz$^{1/2}$/W.

ACKNOWLEDGMENT

This work was supported by the DoD Multidisciplinary University Research Initiative (MURI) program administrated by AFOSR under Grant No. F49620-98-1-0474.

[1] D. Pan, E. Towe, and S. Kennerly, Appl. Phys. Lett. **76**, 3301 (2000).
[2] A. Stiff, S. Krishna, P. Bhattacharya, and S. Kennerly, Appl. Phys. Lett. **79**, 421 (2001).
[3] S. Maimon, E. Finkman, G. Bahir, S. E. Schacham, J. M. Garcia, and P. M. Petroff, Appl. Phys. Lett. **73**, 2003 (1998).
[4] S. Y. Lin, Y. R. Tsai, and S. C. Lee, Appl. Phys. Lett. **78**, 2784 (2001).
[5] Z. H. Chen, O. Baklenov, E. T. Kim, I. Mukhametzhanov, J. Tie, A. Madhukar, Z. M. Ye, and J. C. Campbell, J. Appl. Phys. **89**, 4558 (2001).
[6] Z. M. Ye, J. C. Campbell, Z. H. Chen, E. T. Kim, and A. Madhukar, IEEE J. Quantum Electron. **38**, 1234 (2002); Z. M. Ye, J. C. Campbell, Z. H. Chen, O. Baklenov, E. T. Kim, I. Mukhametzhanov, J. Tie, and A. Madhukar, Mater. Res. Soc. Symp. Proc. **692**, H9.17.1 (2002).
[7] Z. H. Chen, E. T. Kim, and A. Madhukar, J. Vac. Sci. Technol. B **20**, 1243 (2002).
[8] Z. H. Chen, E. T. Kim, and A. Madhukar, Appl. Phys. Lett. **80**, 2490 (2002).
[9] E. T. Kim, Z. H. Chen, and A. Madhukar, Appl. Phys. Lett. **79**, 3341 (2001).

[10] E. T. Kim, Z. H. Chen, and A. Madhukar, J. Vac. Sci. Technol. B **20**, 1188 (2002).
[11] D. Pan, E. Towe, and S. Kennerly, Appl. Phys. Lett. **75**, 2719 (1999).
[12] J. Phillips, P. Bhattacharya, S. W. Kennerly, and M. Dutta, IEEE J. Quantum Electron. **35**, 936 (1999).
[13] O. Baklenov, Z. H. Chen, E. T. Kim, I. Mukhametzhanov, A. Madhukar, F. Ma, Z. Ye, B. Yang, and J. Campbell, The 58th IEEE Device Research Conference, Denver, CO, June 19–21, 2000, p. 171; Z. H. Chen, O. Baklenov, E. T. Kim, I. Mukhametzhanov, J. Tie, A. Madhukar, Z. Ye, and J. Campbell, *Proceedings of QWIP2000 Workshop*, Dana Point, CA, July 2000; Infrared Phys. Technol. **42**, 479 (2001).
[14] Z. M. Ye, J. C. Campbell, Z. H. Chen, E. T. Kim, and A. Madhukar, J. Appl. Phys. **92**, 4141 (2002).
[15] Z. H. Chen, E. T. Kim, and A. Madhukar, Appl. Phys. Lett. **80**, 2770 (2002).